Article

U-Th-He Geochronology of Pyrite from Alteration of the Au-Fe-Skarn Novogodnee-Monto Deposit (Polar Urals, Russia)—The Next Step in the Development of a New Approach for Direct Dating of Ore-Forming Processes

Olga Yakubovich [1,2,*] , Ilya Vikentyev [3,4] , Ekaterina Ivanova [1,2], Mary Podolskaya [5], Ivan Sobolev [3], Eugenia Tyukova [3,6] and Alexander Kotov [2]

[1] Institute of Earth Sciences, Saint-Petersburg University, 199034 Saint-Petersburg, Russia; ekate.s.ivanova@gmail.com
[2] Institute of Precambrian Geology and Geochronology (IPGG), Russian Academy of Sciences, 199034 Saint-Petersburg, Russia; abkotov-spb@mail.ru
[3] Institute of Geology of Ore Deposits, Petrography, Mineralogy and Geochemistry (IGEM), Russian Academy of Sciences, 119017 Moscow, Russia; viken@igem.ru (I.V.); sobolev_id@mail.ru (I.S.); evgtyuk@mail.ru (E.T.)
[4] Engineering Academy, Peoples' Friendship University of Russia (RUDN University), 117198 Moscow, Russia
[5] Vernadsky Institute of Geochemistry and Analytical Chemistry (GEOKHI), Russian Academy of Sciences, 119991 Moscow, Russia; marypodolskaya@gmail.com
[6] Scientific Geoinformation Centre, Russian Academy of Sciences, 119019 Moscow, Russia
* Correspondence: olya.v.yakubovich@gmail.com

Abstract: We report on the application of the U-Th-He method for the direct dating of pyrite from the alteration halo of the Novogodnee-Monto Au-Fe-skarn deposit, Polar Urals. The deposit is genetically related to the formation of volcanogenic complexes of the Ural Paleozoic belt. A modification of the original methodology for measuring U, Th and He isotopes in a single grain allowed us to determine a U-Th-He age of 382 ± 8 Ma (2σ) based on six pyrite samples from the altered rocks of the deposit (U mass fraction ~0.2 mg/kg; Th/U ~3.5; ^{4}He specific volume ~10^{-5} cm^3·STP·g^{-1}). This age is consistent with estimates of the age of ore formation and coeval with the end of the period of island arc magmatic activity. Our results indicate that U-Th-He dating for pyrite samples of ~1 mg in weight from the hydrothermal-metasomatic halo of ore bodies is possible, providing a crucial next step in the development of U-Th-He pyrite geochronology.

Keywords: geochronology; U-Th-He; pyrite; Novogodnee-Monto; Polar Urals; alteration; Au-Fe-skarn deposit; Russia

1. Introduction

In the past decade, a large body of work has been focused on understanding the behavior of radiogenic helium in various minerals that has not been traditionally studied for geochronology, such as hematite, magnetite, calcite, native metals, arsenides and sulfides ([1–7] and references within). Some of these minerals have shown a high retentivity of helium, which may facilitate their use as He-geochronometers [1,3,8], including pyrite. The first application of dating pyrite using the U-Th-He method from the Uzelga VMS-type deposit was successful [8,9]. This success opened up a new perspective for dating ore-forming, sedimentary and tectonic processes, as pyrite is often formed during these processes.

Traditionally, sulfide mineralization has been directly dated by the Re-Os method and in some cases by the Rb-Sr, Sm-Nd and Ar-Ar methods [10–16]. To date, Re-Os geochronology of pyrite has successfully used a large variety of ore deposits, such as orogenic gold, porphyry, sedimentary exhalative and Mississippi Valley-type deposits [11,17–20]. However, the analytical procedures and results obtained from pyrite Re-Os geochronology are

complex, typically showing a high degree of scatter and/or imprecise ages [20–22]. The imprecise ages could be related to isotopic heterogeneity of the trapped Os or by disruption of the Re-Os system by subsequent processes such as metamorphism.

U-Th-He dating of pyrite holds several potential advantages compared to the traditional Re-Os dating technique. Firstly, it requires less material (~1 mg) compared to Re-Os dating (~400 mg). Secondly, the methodology of U-Th-He dating is simpler, and its realization is financially less expensive, as it is based only on the measurement of U, Th and He concentrations. Thirdly, the behavior of osmium during polycyclic ore formation and/or secondary overprinting processes, which are often accompanied by recrystallization/overgrowth of the pyrite, is extremely difficult to quantify. This results in scattering of the Re-Os ages. In the case of the U-Th-He isotope system, the behavior of parent and daughter isotopes exhibits greater contrast compared to other radioisotope systems. Helium is chemically inert, and its response to geologic processes is mainly diffusion controlled. This provides unique opportunities for the dating of geological processes, which are not possible by other techniques, for example, to quantify the timing of recrystallization. Breaking the bonds during the recrystallization provoke He loss when the mobility of other non-inert elements is limited.

Here, we applied the U-Th-He method for the direct dating of pyrite from altered rocks of the Novogodnee-Monto Au-Fe-skarn deposit, located in the Polar Urals, Russia. The Novogodnee mineral field is the largest and most promising one in the entire Polar Urals, with estimated gold reserves of 33 t. Quarrying the deposit over the last 10 years, in preparation for open pit mining, allowed the authors to better study this ore field in terms of the sequence of magmatic processes, hydrothermal alterations and ore mineralization. The goal of this paper is to experimentally test the possibility of U-Th-He dating of pyrite from such ore deposits, promoting the development of an approach for using pyrite as a U-Th-He geochronometer.

2. Isotope-Geochemical Background

The U-Th-He method is based on the accumulation of He atoms produced by the alpha decay of U and Th, which is described by the following equation:

$$^{4}He = 8\,^{238}U\left(e^{\lambda_{238}t} - 1\right) + 7\,^{235}U\left(e^{\lambda_{235}t} - 1\right) + 6\,^{232}Th\left(e^{\lambda_{232}t} - 1\right), \qquad (1)$$

where λ_{238}, λ_{235} and λ_{232} are the decay constants of ^{238}U, ^{235}U and ^{232}Th, respectively. The 8, 7 and 6 coefficients are the amounts of ^{4}He atoms produced by the decay of corresponding parental nuclide.

The detailed isotope-geochemical constraints regarding the possibility of U-Th-He dating of pyrite are described elsewhere [2,8,9]. Here, we briefly summarize the major prerequisites.

1. The mass fraction of parental nuclides of U and Th in the pyrite range from the first ng/kg to first wt.% depends on the type of ore and its locality [23–25]. The positions of U and Th within the pyrite crystal lattice are unclear. Some U and Th may be in micron-size inclusions of U-bearing and/or Th-bearing minerals, such as uraninite, brannerite, monazite, apatite or rutile [26–28]. Alpha particles produced by the decay of U and Th travel from 10 to 20 μm from their parents [29]. It indicates that all radiogenic ^{4}He produced in U-bearing and Th-bearing micron-size inclusions is implanted in the crystal structure of pyrite due to the alpha-recoil effect. It also indicates that the accumulation of radiogenic He by micron size inclusions is physically impossible. Thus, the question of the genetic relationship of the inclusions and pyrite is not applicable. U-Th-He age records the age of pyrite formation rather than the age of the inclusions. A microradiography study has shown that there is another form of U occurrence within pyrite in addition to inclusions, which does not form star-like inclusion-related patterns on the detector [25]. Baranov and Vertepov [25] interpreted such microradiographic patterns as possible evidence of U sorption from the fluid by the pyrite surface during crystal growth. The mechanism of U sorption by pyrite

is described in detail in Reference [30]. In general, the distributions of U and Th in pyrite are strongly heterogeneous [9], requiring the measurement of U, Th and He in the same grain.

2. Specific volume of trapped/hydrothermal fluid-derived He in sulfides do not typically exceed 10^{-8}–10^{-10} $cm^3 \cdot STP \cdot g^{-1}$ [31–35]. Thus, the amount of fluid-derived ^4He may be considered insignificant for samples older than a few tens of millions of years [9].

3. Pyrite has a particularly strong thermal retentivity for ^4He [2]. Step-heating experiments have shown that He begins to migrate from the pyrite crystal lattice at temperatures of ~450 °C, when the mineral begins its transformation into pyrrhotite or magnetite (depending on the amount of oxygen in the system).

All of the above indicate that U-Th-He geochronology could potentially be applied to pyrite. This notion is supported by the first results of U-Th-He dating of pyrite from the VMS-type Uzelga deposit [8,9] and indirectly by successful Pt-He dating of sperrylite ($PtAs_2$) [3], which is its complete crystallographic analog.

3. Object of Study

3.1. Geological Setting

The Au-Fe-skarn Novogodnee-Monto deposit is the first industrial-scale gold body in the Polar Urals (Yamal-Nenets Autonomous Area) [36]. The deposit is located in the south-eastern part of the Toupugol-Khanmeyshor ore district (66°48.81′ N; 66°29.01′ E), which is a constituent of the Voikar zone of the Polar Urals (Figure 1). The Voikar zone is a narrow (a few dozen km) band of Late Ordovician–Middle Devonian volcanic-sedimentary and partly comagmatic plutonic complexes, elongated in a north-north-east direction [37]. Together, they belong to the Polar-Urals paleo-island arc system and the Voikar back-arc basin [38–41].

The ore district is located within a large (8.5 × 7.5 km) asymmetric volcanic-tectonic depression, composed mainly of Silurian–Lower Devonian island-arc basalts and basaltic andesites, volcanic-sedimentary and sedimentary rocks of the Toupugol series (Wenlock–Ludlow), with silty pelitic, psammitic and gravel sizes of volcanic clasts [42–45]. The volcanic-sedimentary series form a monocline, complicated by a series of bends with a dip towards the south-east (Figures 2 and 3). These stratified rocks are located in the roof of the Late Silurian–Middle Devonian comagmatic, multiphase gabbro-diorite-plagiogranite Sob' (Lagorta-Kokpela) batholith [38,41,44–48]. The ore district is located in a long-lived tectonic zone forming a series of faults oriented in a north-west direction, which are recognized as some of the key conduits for various types of ore mineralization [46,49–52].

The Novogodnee-Monto deposit is located in the exocontact zone of the large diorite stock of the Sob' complex and is hosted by predominantly metabasalts, basic volcanoclastic rocks and limestones of the Toupugol series [45–47] (Figure 4). At the Novogodnee-Monto deposit and in its vicinity, younger Early Carboniferous rift-related basite intrusions (dolerite sills, monzodiorite and lamprophyre dykes) are also identified [50]. These bodies belong to the Musyur (Malyi Khanmey) hypabyssal complex (Figures 2 and 3). Their formation was associated with the accretion by the Polar Ural island arc and formation of the Early Uralian orogen [48,50].

3.2. Types of Gold Mineralization

The Novogodnee gold field contains several different types of ore mineralization, which are superimposed on each other and distributed across a relatively small area of 2.5 km^2. Based on the morpho-structural features of the deposit, there are two industrial types of Au-bearing mineral assemblages: (1) gold-sulfide-magnetite ore confined to skarn-magnetite bodies; and (2) veinlet-disseminated gold-sulfide-quartz ore, associated with zones of propylitization (epidote–chlorite–sericite–secondary albite assemblage ± calcite) and pyrite-sericite-quartz alteration [45].
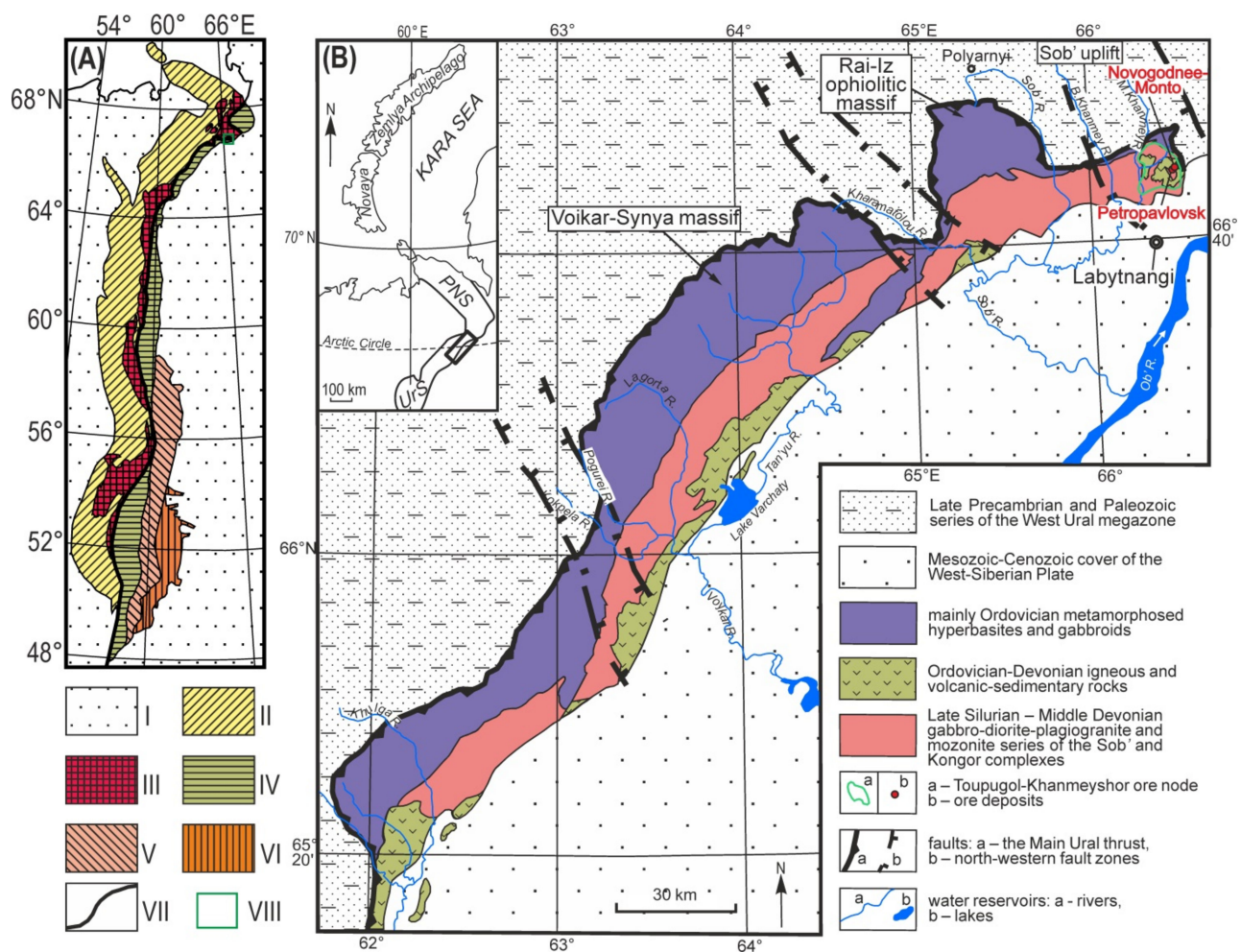
Figure 1. Location maps. (**A**) Tectonic scheme of the Ural fold belt based on the geological map in [42]; I—Mesozoic–Cenozoic complexes of the East European platform and West Siberian plate; II, III—Paleozoic complexes of the Western Urals (II) and Precambrian (III); IV—Early–Middle Paleozoic complexes of the Tagil-Magnitogorsk megazone; V—Precambrian and Paleozoic complexes of the East Uralian megazone; VI—Paleozoic and Precambrian complexes of the Trans-Urals; VII—Main Ural fault; VIII—position of the Toupugol-Khanmeyshor ore district of the Polar Urals. (**B**) The position of the Toupugol-Khanmeyshor ore district in the structures of the Polar Urals was compiled using data from [38,39]. PNS and UrS (on the inset)—Paykhoy-Novaya Zemlya and Ural folding-thrust structures.

The *gold-sulfide-magnetite* type of mineralization is associated with skarn and skarn-magnetite quasi-conformable lenses, located above the diorite massif at the contact point between limestone and tuff-sedimentary rocks. The ore bodies are represented by complicated lenses reaching thicknesses of several tens of meters. The ore structures are massive, banded-spotted and occasionally spotty-disseminated. This type of mineralization is directly associated with intrusion of the diorite of the Sob' plutonic complex. Ore minerals are represented by magnetite, pyrite, minor chalcopyrite and rare cobaltite, pyrrhotite, arsenopyrite, marcasite and native gold. The occurrence of gold minerals is controlled by pyrite defects, and they are occasionally associated with chalcopyrite cementing pyrite. In general, native gold corresponds to low-fineness gold (76.0–88.0 at. %), however, if it is associated with cobaltite and Co-bearing pyrite and chalcopyrite, its fineness increases to 90.0–99.0 at. % [51].

Gold-sulfide-quartz mineralization mainly corresponds to pyrite-sericite-quartz alteration. Thin gold-bearing steeply dipping quartz and carbonate-quartz veins and linear stockworks are confined to fault zones. Ores of this type comprise steeply and sub-vertically dipping thin vein disseminated mineralization zones. The thickness of the Au-sulfide-quartz ore bodies is variable and ranges from 1 to 10 m, with average C_{Au} = 3.7 g/t [43]. The

mineral assemblage of this ore type is pyrite, with minor galena, sphalerite, chalcopyrite and hematite. Small occurrences of native gold (up to 20 μm) are associated with pyrite and galena, rarely with chalcopyrite, and sometimes they occur in quartz or chlorite [36]. Gold fineness is rather low (83.0–86.0 at. %) [45].

3.3. Hydrothermal Metasomatic Alterations

Within the deposit, alteration haloes are the result of skarn, propylitization and beresitization processes [52]. Based on the results of Rb-Sr dating of quartz-sericite alteration [52,53], V.V. Kenig and K.V. Butakov concluded that the processes of metasomatism and ore formation occurred between 360 and 400 Ma [49]. Infiltration calcareous skarns were formed at the contacts between mafic volcanic rocks and limestones or carbonate-bearing volcaniclastic rocks. Therefore, their formation is tectonically and lithologically controlled. The skarns are located in the supra-intrusive part of the diorites of the Sob' complex. Due to the morphology of the pluton, the skarn bodies have a lenticular-ribbon shape in terms of cross section and correspond to the pyroxene-garnet-epidote facies. The last stage of skarn formation was magnetite mineralization, and massive magnetite bodies formed as a result. They host inclusions of pyrite and other ore minerals, along with minor late gold mineralization. The thickness of the alteration aureoles reaches tens of meters.
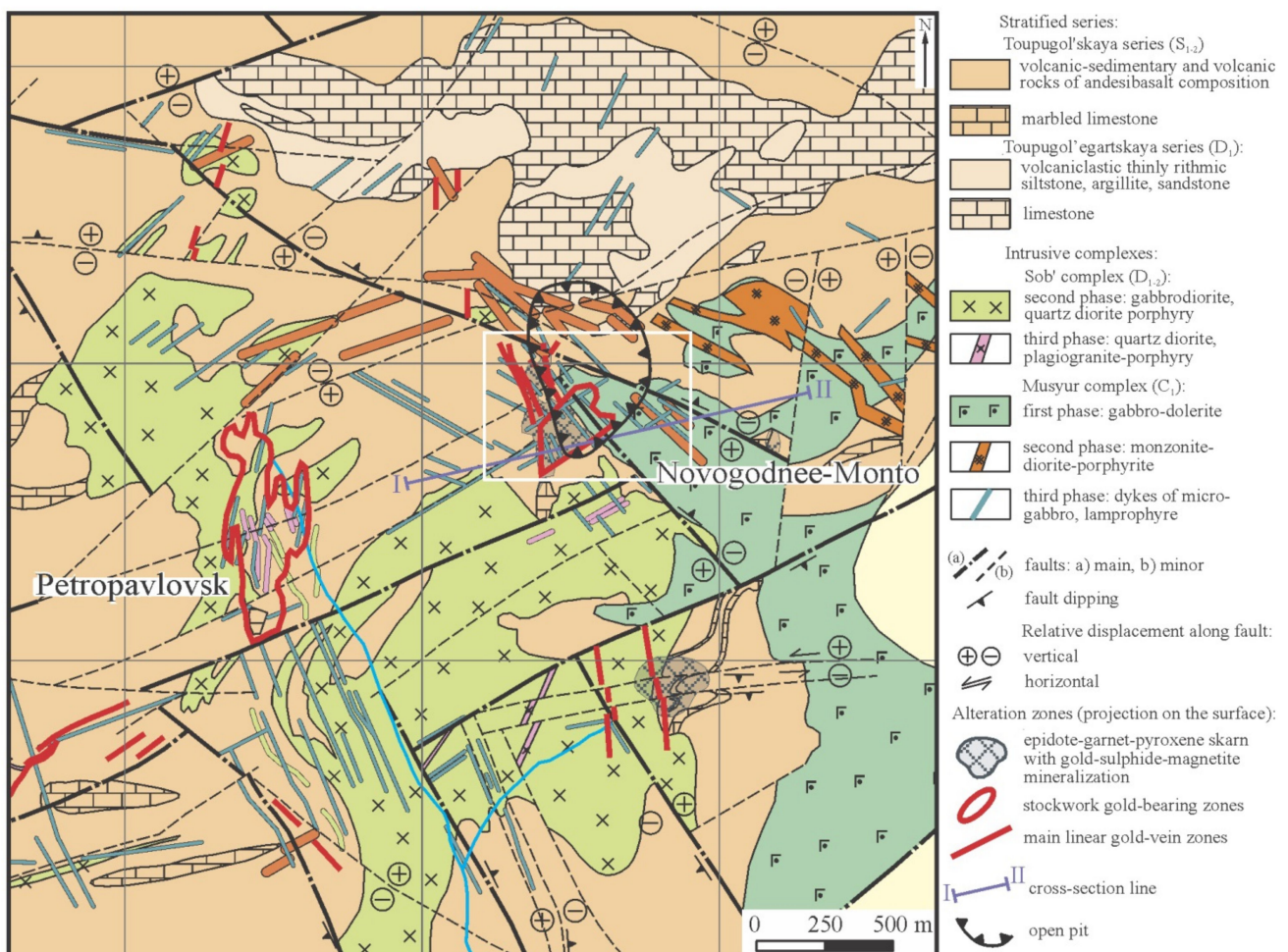

Figure 2. Geological map of the Novogodnee gold field, compiled using data in Reference [43] and JSC "Yamalgold", simplified after [45]. The white box outlines the boundaries of the geological map illustrated in Figure 4.
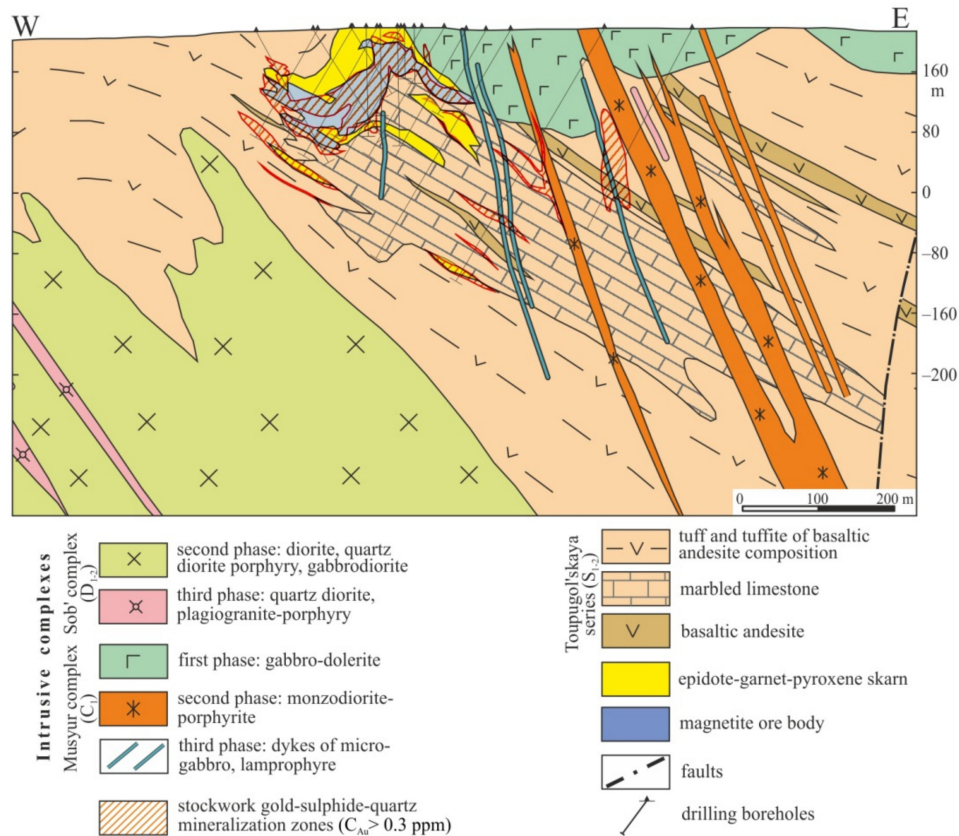
Figure 3. Geological cross-section of the Novogodnee-Monto gold-iron deposit along line I–II on Figure 2, compiled using data in Reference [43] and JSC "Yamalgold", simplified after [45].

Figure 4. Geological scheme of the Novogodnee-Monto deposit. The labelled yellow dot indicates the sampling location (NM-17), was compiled using data from [46].

The propylitization process is represented by epidote-chlorite, carbonate-chlorite and actinolite-epidote facies in the outer zones of the skarn. It should be noted that

representative epidote-chlorite alteration forms haloes on a larger scale of up to 100 m, including across the endocontacts of the di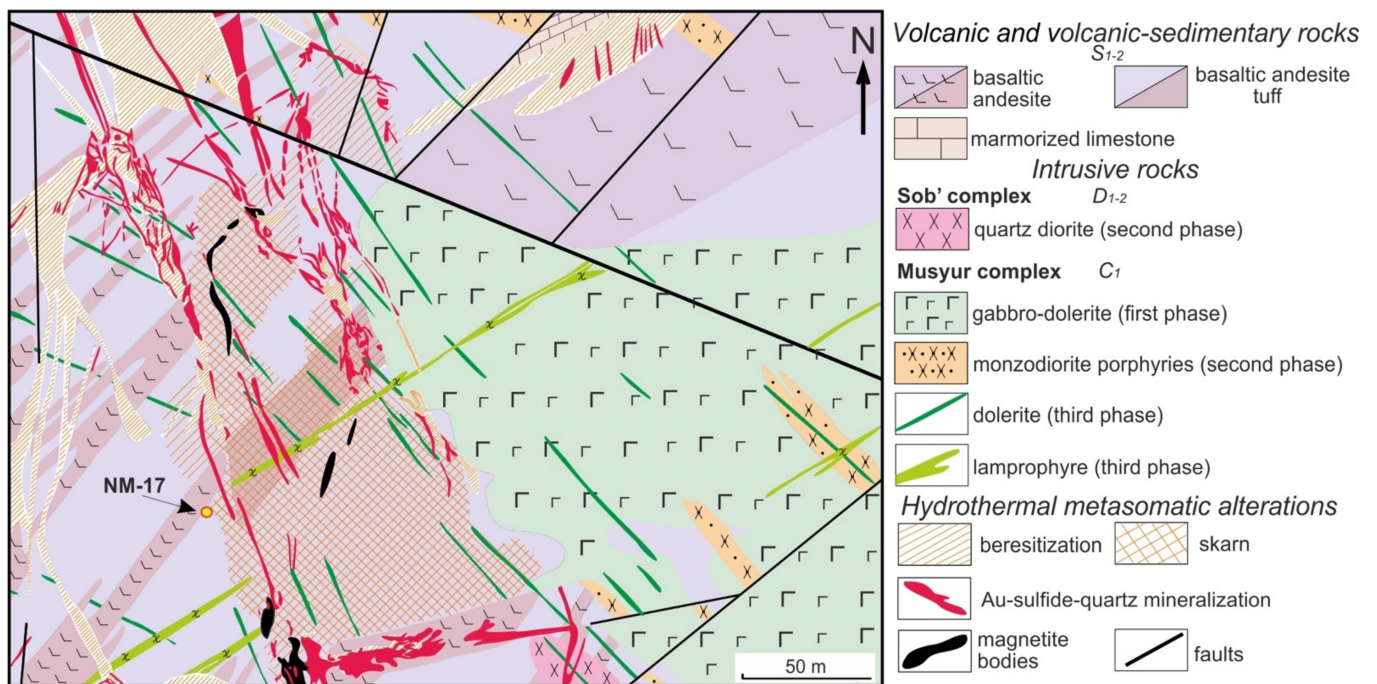orite massif. In contrast, actinolite-epidote rocks are confined to fractures oriented in submeridional and north-eastern directions. The propylitization zones reach lengths of hundreds of meters and thicknesses of tens of meters.

The processes of beresitization (sericite-Ca-Mg-carbonate-pyrite-quartz alteration) occurred during the subsequent late hydrothermal stage, when north-south-oriented alteration zones were formed [52]. These beresite-like altered rocks are associated with gold-sulfide-quartz mineralization, which is mainly represented by thin quartz and quartz-carbonate veins, comprising linear vein-veinlet Au-Ag-sulfide-quartz systems (Figure 4). In the regional scale, the distribution of alteration zones is controlled by submeridional to north-west striking fault systems (Figure 4). The thicknesses of the beresite-like alteration zones reach several tens of meters, with average length of hundreds of meters.

3.4. The Age of Mineralization

Mineralization within the Novogodnee-Monto gold-iron-skarn deposit is associated by most researchers with the Early–Middle Devonian stage of granitoid magmatism, but little direct evidence has been presented ([45] and references therein). Published estimations for the age of ore mineralization range from the Silurian to the Triassic and are mainly based on geological relationships between sedimentary and magmatic rocks [46,49,52,54,55]. Paleotectonic and paleogeodynamic reconstructions are also complicated by the limited number of reliable geochronological data obtained for magmatic complexes and sedimentary series [39,48].

Several ore-formation stages may be reconstructed in the Toupugol-Khanmeyshor mineral district [52,54,56]. All of them are believed to be related to the evolution of the Polar-Ural paleo-island arc [45,57].

The Novogodnee ore field was formed in a mature island-arc tectonic setting during two stages. The early stage was associated with the submarine formation of lavas and accumulation tuffs of the basalt-andesibasalt composition and the associated minor sedimentary strata (Toupugol suite, S_{1-2}). The volcanic-sedimentary deposition of scattered and mainly stratiform pyrite mineralization, with a geochemical association of Co-Ni-Cu-Zn-Ag-Au, was synchronous with calc-alkaline volcanism [45]. The late volcanic stage was closely associated with the accumulation of sedimentary and minor volcaniclastic units of the basalt-andesite and trachybasalt-andesite series (Toupugol'egart suite, D_1). These rocks are cross-cut by younger intrusions of the gabbro-diorite-plagiogranite Sob' complex (D_{1-2}) and the late-stage gabbro-dolerite dykes of the Musyur complex (C_1) [40,45,50]. The geological structure and ore deposits of the Novogodnee mineral field were studied from 1957 [46,51,52,54,58,59]. The U-Pb ages of zircons from diorites of the second (main) and plagiogranites of the third phases of the Novogodnee gold field are 410 ± 2 Ma [45] and 403 ± 4 Ma [40]. The $^{40}Ar/^{39}Ar$ age of plagioclase from diorites of the main phase of the same region is 414 ± 30 Ma [40], which supports the more reliable U-Pb dates.

Ore deposit formation was associated with the intrusion and cooling of diorites and plagiogranitoids of the Sob' complex, and the process occurred in two major stages: (1) high-temperature—skarn stage (D_{1-2}); and (2) low-temperature—beresite stage (D_{2-3}) [45]. The pyrite-sericite-quartz assemblage of the later stage (Figure 5) was superimposed on the earlier generations of hydrothermal-metasomatic alterations. The age of the beresite-like alterations can be correlated with the final stage of granitoid magmatism in the Polar Urals. The dating of sericite from such low-temperature gold-bearing alteration by the $^{40}Ar/^{39}Ar$ method yields a crystallization age of 382 ± 4 Ma [60]. The Rb-Sr age of quartz-calcite-sericite-chlorite alteration in the Novogodnee field has been determined as 360 ± 1 Ma [52,53].
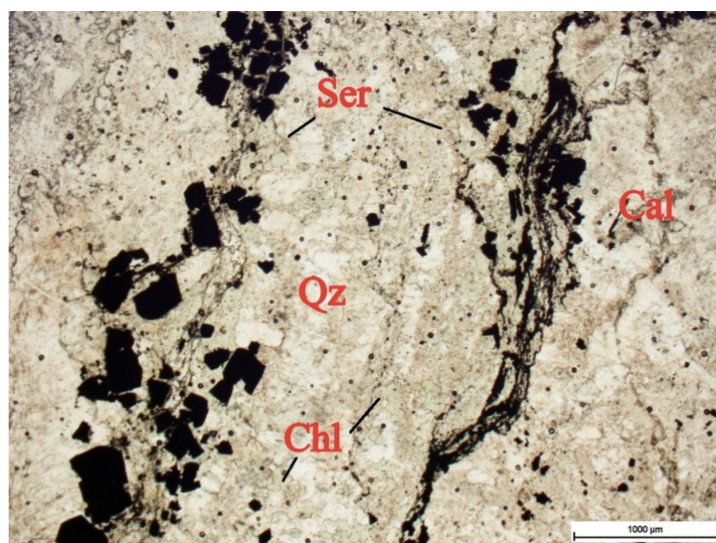
Figure 5. Gold-bearing pyrite-sericite-quartz alteration of the Novogodnee-Monto deposit in thin section of sample NM-19. Pyrite from the same type of rock nearby was used for U-Th-He dating. Qz—quartz; Chl—chlorite; Ser—sericite; Cal—calcite.

4. Analytical Methods

The pyrite grains were separated from the rock using bromoform ($CHBr_3$)-based heavy liquid separation techniques at the Institute of Geology of Ore Deposits, Petrography, Mineralogy and Geochemistry (Russian Academy of Sciences, Moscow, Russia). For U-Th-He dating, pyrite grains without any visible inclusions were picked under the binocular microscope. Three to ten cubic-shaped grains were used for each measurement. The average grain size ranged from ~200 to 500 µm, with total sample weights of 1–2 mg. Prior to U-Th-He dating, pyrite grains from the same rock in polished sections were studied on a Hitachi S-3400N scanning electron microscope (Tokyo, Japan) equipped with an AzTec Energy 350 detector (Abingdon, UK) at the "Geomodel" Research Centre (Saint-Petersburg State University, Saint-Petersburg, Russia) and on JSM-5610LV with JED-2300 EDS (Tokyo, Japan) at the Center for Collective Use IGEM-Analitika (Institute of Geology of Ore Deposits, Petrography, Mineralogy, and Geochemistry, Russian Academy of Sciences, Moscow, Russia).

4.1. Measurement of Radiogenic ^{4}He Contents

The ^{4}He contents were measured at the Institute of Precambrian Geology and Geochronology (Russian Academy of Sciences, Saint-Petersburg, Russia) with a high-sensitivity MSU-G-01-M mass spectrometer (Saint-Petersburg, Russia). For each measurement, 3–10 pyrite grains attaining a total weight of ~1–2 mg were placed in a quartz ampoule (~1 cm long) and sealed under vacuum conditions (10^{-3} torr). By using a special lock, the ampoule was transported into a Re cylinder and heated in several steps up to temperatures of ~1100 °C. The first step included 30 minutes at a temperature of 200 °C to remove any remaining atmospheric ^{4}He and to significantly reduce the He blank. Details of the He measurement technique and the design of the instrument are described in References [1,9,61]. The total procedural blank, determined by heating the empty quartz ampoule in the Re cuvette to 1100 °C, corresponds to ~5×10^{-10} cm^3·STP, whereas the detection limit of the instrument is ~5×10^{-13} cm^3·STP of ^{4}He. Preheating reduces the He blank by five times to ~1×10^{-10} cm^3·STP. Following the extraction of He, the ampoule was removed from the mass spectrometer for the subsequent separation of U and Th.

4.2. Measurement of U and Th Contents

We have improved the pyrite dissolution protocol compared to the previously suggested method in Reference [9]. A portion of the U and Th in sulfides may occur in

micron-sized mineral inclusions. We have performed a set of pyrite dissolution experiments, which revealed that some of these mineral inclusions remain undissolved if HF is not used in the dissolution process. We therefore recommend the use of HF for complete dissolution of pyrite grains.

The quartz ampoule with degassed samples was spiked with a ^{230}Th-^{235}U tracer and dissolved in a mixture of an aqua regia digest (1 mL), concentrated hydrofluoric acid (0.5 mL) and perchloric acid (0.05 mL) in closed Teflon vials for 24 h at a temperature of 130 °C. The solution was dried on a hot plate at 200 °C in order to prevent the formation of fluorine-based complexes. Dissolution of a quartz ampoule (weight ~40–50 mg) significantly increases the salinity of the solution. However, prolonged heating in the presence of hydrofluoric acid will vaporize most of the silica in the SiF_6 form. The remaining precipitate was dissolved in 1.5 mL of 5% nitric acid for further measurements of the ^{235}U/^{238}U and ^{230}Th/^{232}Th isotope ratios on an ELEMENT XR ICP mass-spectrometer (Bremen, Germany) in Vernadsky Institute of Geochemistry and Analytical Chemistry, Russian Academy of Sciences, Moscow, Russia.

The accuracy of the complete dating procedure (measurement of He, U and Th) was assessed by simultaneous experiments on a Durango apatite, which is the international standard for the U-Th-He method.

5. Results

5.1. Mineralogical Features

Scanning electron microscope (SEM) analysis of the pyrite grains revealed the presence of micron-sized inclusions of gold, galena, hessite and arsenopyrite (Figure 6). The chemical composition of the pyrite grains is presented in Table 1.
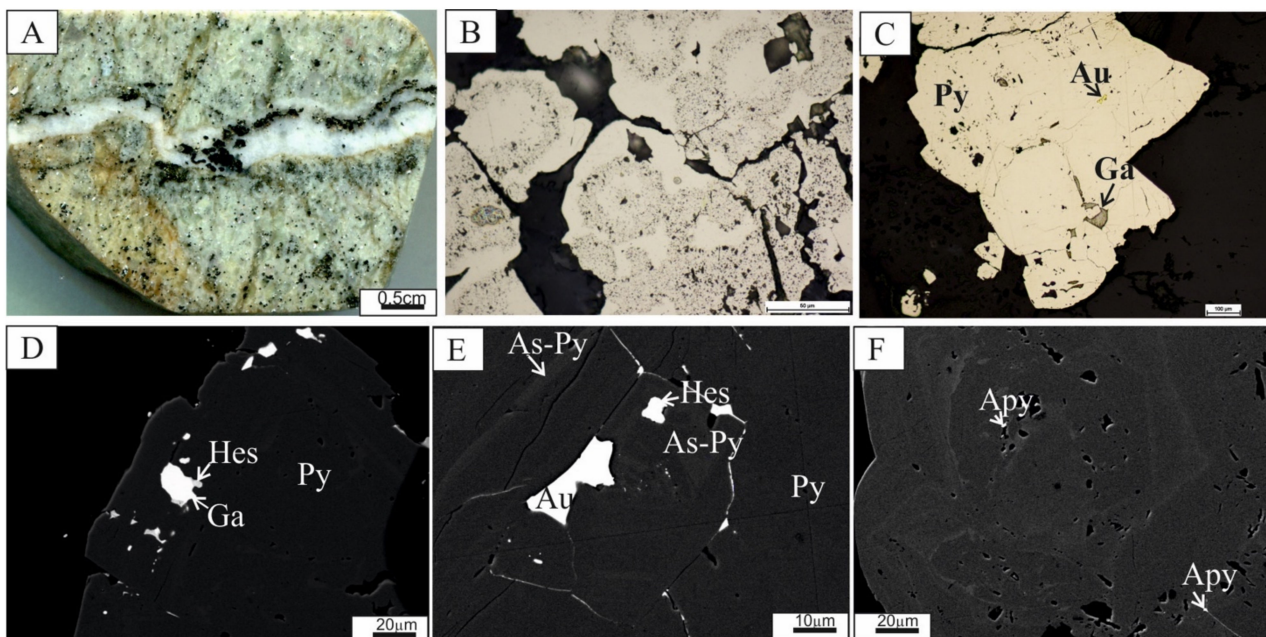

Figure 6. Pyrite-quartz-sericite alteration. (**A**) Metasomatic sulfide-quartz vein with zonal distribution of sulfide inclusions; (**B**) zonal distribution of host rock inclusions in pyrite (Py) metacrystals; (**C**) micro-inclusions of native gold (Au) and galena (Ga) along the boundaries of pyrite crystals; (**D**) linearly distributed micro-inclusions of galena and hessite (Hes) in a pyrite crystal; (**E**) zonal block of arsenic-containing pyrite (As-Py) with inclusions of native gold and hessite; (**F**) the fine-zoning structure of As-pyrite with small arsenopyrite (Apy) inclusions in the more arsenic-rich zones. (**D–F**) Scanning electron microscope (SEM and BSE) images of selected pyrite grains by JSM-5610LV with JED-2300 EMF (Tokyo, Japan), analyst N.V. Trubkin, IGEM RAS.

Table 1. Chemical composition of pyrite, wt%.

Sample	S	Fe	As	Σ	Formula
NM-17	52.43	45.40	<0.05	97.83	$Fe_{0.98}As_{0.0}S_{2.02}$
	51.21	44.65	1.94	97.80	$Fe_{0.98}As_{0.032}S_{1.99}$
	52.33	46.17	2.73	101.23	$Fe_{0.98}As_{0.044}S_{1.98}$

The analyses were performed by JSM-5610LV with JED-2300 EDS (Tokyo, Japan) analyst N.V. Trubkin (IGEM RAS).

5.2. U, Th and He Measuring Results

The results of the U, Th and He concentration measurements are presented in Table 2. We performed six measurements of pyrite from the NM-17 location in total. We dated ~70 pyrite grains in total, since each of the six samples was composed of numerous pyrite grains.

Table 2. Results of U-Th-He dating of pyrite from the Novogodnee-Monto deposit.

Sample Number	Sample ID	U, 10^{10} at	σ	Th, 10^{10} at	σ	Th/U	^{4}He, 10^{10} at	σ	T, Ma	σ
NM-17	872	17.7	0.5	82.3	2.0	4.8	17.8	0.3	370	8
NM-17	875	54.8	1.4	138.0	3.2	2.5	42.0	0.4	368	6
NM-17	877	34.1	0.9	128.6	4.1	3.8	34.0	0.4	405	7
NM-17	878	44.5	1.9	173.0	6.6	3.9	41.7	0.6	376	10
NM-17	889	51.4	2.9	208.8	2.6	4.1	51.2	0.3	391	12
NM-17	890	42.7	1.2	181.7	3.2	4.3	46.4	0.4	417	7
"pooled" *		186.7	2.0	186.7	2.0	3.8	202.5	7.6	383	8
							central age		382	4
Qu blank		0.9	0.6	2.4	1.5		0.4	0.3		

* Sample 890 was excluded from the calculation of the pooled and central ages as it was considered anomalous.

The specific volume of ^{4}He in pyrite grains were ~10^{-5} cm^3·STP g^{-1}. ^{4}He was released from all samples when pyrite decomposed into pyrrhotite and sulfur at ~500 °C. Measured ^{4}He specific volumes are greater than the typical values for trapped/hydrothermal fluids (10^{-8}–10^{-10} cm^3·STP·g^{-1}). U mass fraction ranged from 0.1 to 0.5 mg/kg, while the average Th/U ratio was ~3.5.

5.3. Calculation of the U-Th-He Age

The U-Th-He age was calculated using the Helioplot (ver. 2.1) and IsoplotR software (ver. 4.2) [62]. The average U-Th-He age can be calculated with different methods, including (1) the arithmetic mean of the single-grain ages; (2) the "pooled" age; (3) the U-Th-He isochron age; and (4) the central age. From a mathematical viewpoint, the latter method is the most accurate [63] (Table 2; Figure 7).
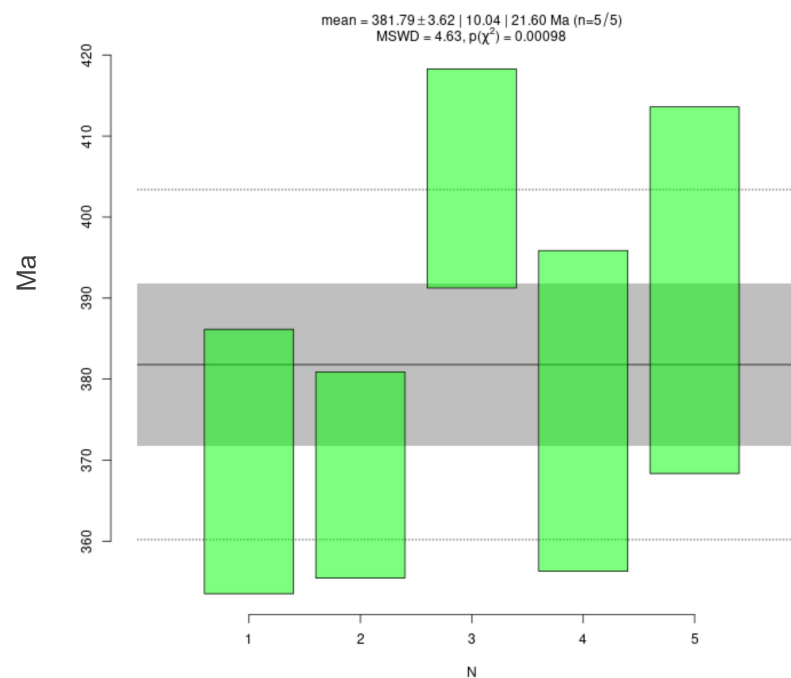
Figure 7. Weighted mean plot for pyrite from the Novogodnee-Monto deposit, constructed in the IsoplotR software ver. 4.2.

6. Discussion

The central age calculated for the five pyrite samples is 382 ± 8 Ma (2σ). The age of pyrite from the Novogodnee-Monto deposit is consistent with independent geological estimates for the age of ore formation (380–400 Ma). The pyrite U-Th-He ages are quite reproducible but show scattering within the range of 370–420 Ma, which may be explained by (1) the presence of excess ^{4}He, (2) the loss or input of U, Th or He at some point during the sample's geological history, (3) methodological imperfections, or (4) multistage formation of pyrite. It is possible that sample NM-17 contains pyrite of two generations, the first of which corresponds to the skarn stage of formation of the Novogodnee-Monto deposit (about 400 Ma), and the second pyrite generation corresponds to a lower-temperature—beresite stage (382–360 Ma).

6.1. Excess ^{4}He

There could be several explanations for an excess of ^{4}He in minerals, including (1) trapped hydrothermal ^{4}He, (2) excess of ^{4}He in inclusions, or (3) implanted radiogenic ^{4}He:

1. The measured specific volume of ^{4}He in pyrite are several orders of magnitude higher (10^{-5} cm^3·STP·g^{-1}) than ^{4}He specific volumes in hydrothermal sulfides (10^{-8}–10^{-10} cm^3·STP·g^{-1}) [31–35]. In rare cases, the concentrations of trapped hydrothermal He can be higher, up to 10^{-6} cm^3·STP·g^{-1} [64]. In this rare case, the specific volume of trapped hydrothermal He may increase the apparent U-Th-He age by 10%.

2. The alteration temperature was significantly higher than the closure temperature for the U-Th-He isotope system of most minerals [4]. Taking into account that the only observed inclusions in pyrite from the Novogodnee-Monto deposit were composed of quartz, it is very unlikely that inclusions contributed a significant amount of excess ^{4}He in these samples.

3. The calculation of U-Th-He ages requires alpha-recoil corrections [29]. The studied pyrite grains range in size from 200 to 500 μm. Assuming a cubic shape and average alpha-stopping distance of 14 μm (SRIM calculations; [65]), less than 4% of the He can be lost due to the alpha-recoil effect [29].

The mass fractions of U and Th in pyrite are relatively low (0.1–0.5 mg/kg), but they are higher in the surrounding rocks. As a result, implanted [4]He should be taken into account. If we assume U and Th mass fraction of 1 and 3 mg/kg, respectively, within the surrounding host rocks (averages for island arc andesites, volcaniclastic sediments and carbonates; GERM database) and a density of 2.65 g/cm^3, the amount of implanted and ejected He would be practically equal. The amount of implanted He may be more significant if U and Th mass fractions in the surrounding country rock are higher. However, as suggested by References [29,66], the implantation of radiogenic He should result in low reproducibility of the U-Th-He ages due to the highly heterogeneous distribution of U and Th within the surrounding rocks. As the Novogodnee-Monto pyrite grains produced very reproducible ages, excess [4]He is unlikely.

6.2. U-Th-He System Behavior in Pyrite

The open behavior of the U-Th-He system can be related to U and Th input/loss or He loss. Radiogenic He was only released from the studied samples at high temperatures during pyrite decomposition (>450 °C), indicating a high retention of radiogenic He in pyrite. However, the retention of U and Th in the pyrite grains is less clear. Experiments with pyrite from the Uzelga deposit have shown that the interaction of pyrite with weak acids may result in U loss [9]. Pyrite grains used for U-Th-He dating in our study did not show any evidence of oxidation or alteration, which may be expected if long-term contact with slightly acidic mine waters or the atmosphere had occurred. Furthermore, the grains were separated from freshly exposed rock fragments in an open pit. Therefore, it is unlikely that the pyrite U-Th-He system has been recently disturbed.

Pyrite can undergo recrystallization under dynamic and thermal metamorphic events [67–69]. There are currently no data available concerning the behavior of the U-Th-He system during pyrite recrystallization. However, there is only evidence for low-grade metamorphism of the Novogodnee-Monto deposit up to zeolite facies [37]. Low-grade metamorphism up to prehnite-pumpellyite facies did not appear to reset the U-Th-He isotope system in the Uzelga deposit [9].

6.3. Methodological Imperfections

The main methodological complications that could result in scattering of U-Th-He ages are the incomplete release of He from pyrite grains and incomplete pyrite decomposition. [4]He was released from the pyrite grains at ~1100 °C, which is sufficiently hot for releasing all He from pyrite [2]. The pyrite grains were dissolved in a mixture of HF, HClO$_4$ and aqua regia acids (see Section 4.2), which should dissolve most of the U-bearing and Th-bearing minerals.

6.4. Natural Scattering of U-Th-He Ages

Pyrite U-Th-He ages from the Novogodnee-Monto deposit show relatively large scattering between 370 and 420 Ma. There is no correlation between age and concentrations of U, Th or He in the grains (Figure 8). This indicates that it is very unlikely that trapped or implanted He is responsible for the scattering of U-Th-He ages, as the influence of trapped He is concentration dependent.

All U-Th-He ages fall within the timeframe of magmatic and metasomatic activity related to the formation of the volcano-plutonic belt in this region (360–414 Ma; see Section 3.4). Since the pyrite grains display a zonal structure (Figure 6), relatively large scattering of the U-Th-He ages could be related to different phases during ore genesis and crystallization of pyrite. Previous studies of the Kondyor isoferroplatinum deposit have shown that scattering of Pt-He ages between 110 and 145 Ma can be correlated with polycyclic mineral formation [70]. Several generations of pyrite formation are described within the Novogodnee-Monto deposit as well, which potentially could be separated in time. The answer to this question at the moment remains unclear as it is not currently possible to date different growth zones within the pyrite grains.
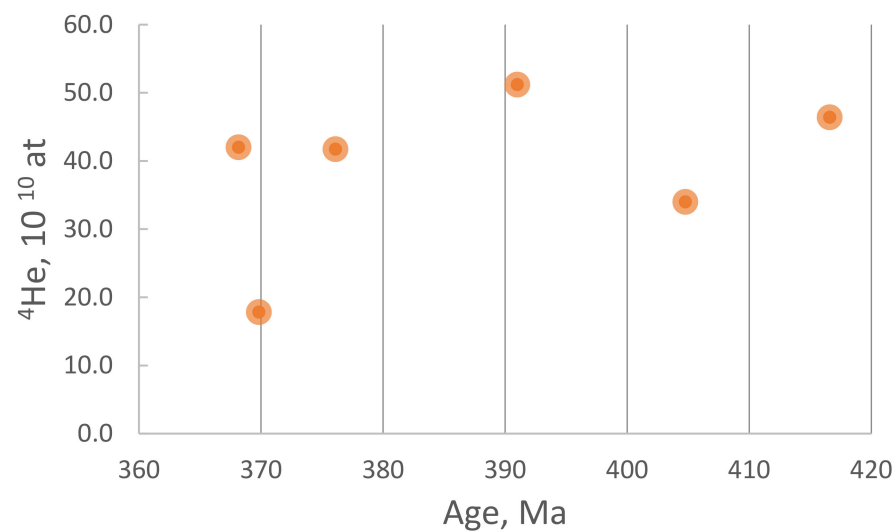
Figure 8. Absence of relationship between He amount of He and U-Th-He age for samples from the Novogodnee-Monto deposit.

6.5. Comparison of Pyrite U-Th-He and Geological Ages

The U-Th-He age of pyrite from the Novogodnee-Monto deposit (382 ± 8 Ma) is supported by independent geological observations. The age of mineralization within the Novogodnee-Monto gold-iron-skarn deposit is associated by most researchers with Early–Middle Devonian granitoid magmatism ([45] and references therein), corresponding to the main stage of diorite magmatism in the Polar Urals. At the final stage of subduction, at the end of the Middle Devonian (387–383 Ma), small granitoid intusives of the Yanaslor complex were formed in the Voikar zone [71–73]. Rb-Sr isochronous ages for the youngest monzodiorite porphyry dykes (382 ± 10 Ma; Eifelian–Frasnian) and ore quartz-calcite-sericite-chlorite alteration (360 ± 1 Ma, Famennian) are younger [52,53]. According to our data [50], these monzodiorite porphyry dikes are somewhat younger and belong to the Musyur complex, whose rocks were formed in the Early Carboniferous (349 ± 3, 347 ± 9, 339 ± 4, 334 ± 3 Ma) at the stage of accretion of the island-arc system to Arct-Lavrussia.

^{40}Ar/^{39}Ar dating of the sericite monofraction from low-temperature gold-bearing alteration in the neighboring gold-porphyry Petropavlovsk deposit yielded a crystallization age of 382 ± 4 Ma [60]. This date can be interpreted as the upper age limit for gold mineralization. The final death of the magmatic chambers that formed the granitoid bodies of the Sob' batholith was reflected in the processes of gold and Cu-Fe (+Au) formation [45,74].

6.6. Questions Regarding the U-Th-He Dating of Pyrite

Our results indicate that U-Th-He dating of pyrite from hydrothermal metasomatic rocks is possible. Alteration of the Novogodnee-Monto deposit is a second example of successful application of analytical procedures for the study of the U-Th-He system in pyrite. The pyrite grains used in this study have different U and He concentrations, Th/U ratios and grain sizes compared to the first successfully dated pyrite from the Uzelga deposit [9]. This is an important step in the development of this dating technique, including a modification from the previously proposed methodology [9].

However, several theoretical and practical problems remain. The reason behind the scattering of U-Th-He ages is still unclear. Pyrite U-Th-He ages from both the Uzelga and Novogodnee-Monto deposits show relatively large scatter across a time interval of around 50 million years. This scatter could be related to both methodological or theoretical imperfections, such as an underestimation of trapped He or incomplete pyrite decomposition. However, this scattering could instead indicate a complex history of pyrite formation, accompanied by sulfide recrystallization. Therefore, this scattering could provide important information which may aid our understanding of the ore-forming processes in these

deposits. These implications could also be applied to understand the "scattering" of Re-Os ages in sulfides.

As previously described, pyrite is a tricky mineral which is not usually used for geochronology. By analogy with zircon, pyrite may contain inherited cores that are "cemented" by a younger pyrite generation. This younger pyrite generation could be associated with tectonics, magmatism, sedimentary basin evolution or biological activity. Therefore, U-Th-He dating of single pyrite grains and/or understanding the processes that disturb the U-Th-He system may provide vital missing information for constructing the geological history of an economic ore deposit.

7. Conclusions

The possibility of U-Th-He dating of pyrite is shown by an example of the altered rocks of the Novogodnee-Monto deposit, Polar Urals. U-Th-He dating of 70 pyrite grains separated into six aliquots yields reproducible ages with an average of 382 ± 8 Ma (2σ). This value is very similar to independent age estimates for the ore-bearing hydrothermal activity within this gold field (~380 Ma). This is the second example of the successful application of the U-Th-He isotope system for dating pyrite, but it is the first successful application for directly dating pyrite from altered rocks. Therefore, our work provides a crucial next step in the development of the U-Th-He dating technique. However, there are still a lot of questions that have to be solved to make this technique widely applicable and reliable. Thus, the U-Th-He system in pyrite has the potential to be a useful tool for the geochronology of numerous geological processes accompanying sulfide crystallization.

It should be emphasized that for many types of ore mineralization formed at low and or moderate temperatures, there are no reliable mineral geochronometers. Rather, they are nominally present, but the impossibility of obtaining their monomineral fractions (due to thin mutual intergrowths) or the small size of individual grains renders reliable isotope dating impossible. Pyrite, which has a relatively high degree of crystallinity, usually forms fairly large crystals even in low-temperature mineral associations. This allows us to consider the prospects for using direct dating methods of pyrite as quite encouraging.

The areas of potential application of this method include a very wide range of areas of ore geology and, in general, economic geology, especially in the field of deciphering the sequence of mineral formation in long-lived ore-forming systems, dating solid sulfide ores and dating the lowest-temperature hydrothermal processes. It is very tempting to use pyrite dating in an area that seems far from ore geology, such as low-temperature geochronology of sedimentary and low-temperature metamorphic rocks, for example, the study of the age of epi-/catagenesis in thick oil-bearing sedimentary units of deep epicratonic depressions—the marginal areas of young and ancient platforms adjacent to orogenic areas. Filling these depressions with oil-producing and gas-producing strata containing scattered carbonaceous matter usually involves abundant pyrite impregnation, the study of the radioisotope system of which will allow dating epigenetic processes associated with oil/gas formation.

References

1. Shukolyukov, Y.A.; Yakubovich, O.V.; Mochalov, A.G.; Kotov, A.B.; Sal'nikova, E.B.; Yakovleva, S.Z.; Korneev, S.I.; Gorokhovskii, B.M. New Geochronometer for the Direct Isotopic Dating of Native Platinum Minerals (190Pt-4He Method). *Petrology* **2012**, *20*, 491–505. [CrossRef]
2. Yakubovich, O.V.; Gedz, A.M.; Vikentyev, I.V.; Kotov, A.B.; Gorokhovskii, B.M. Migration of Radiogenic Helium in the Crystal Structure of Sulfides and Prospects of Their Isotopic Dating. *Petrology* **2019**, *27*, 59–78. [CrossRef]
3. Yakubovich, O.V.; Mochalov, A.G.; Sluzhenikin, S.F. Sperrylite (PtAs2) as a 190Pt-4He Geochronometer. *Dokl. Earth Sci.* **2015**, *462*, 88–90. [CrossRef]
4. Reiners, P.W.; Carlson, R.W.; Renne, P.; Cooper, K.M.; Granger, D.E.; McLean, N.M.; Schoene, B. The (U–Th)/He System. In *Geochronology and Thermochronology*; John Wiley & Sons: Hoboken, NJ, USA, 2017; pp. 291–363.
5. Shuster, D.L.; Vasconcelos, P.M.; Heim, J.A.; Farley, K.A. Weathering Geochronology by (U-Th)/He Dating of Goethite. *Geochim. Cosmochim. Acta* **2005**, *69*, 659–673. [CrossRef]
6. Evans, N.J.; Byrne, J.P.; Keegan, J.T.; Dotter, L.E. Determination of Uranium and Thorium in Zircon, Apatite, and Fluorite: Application to Laser (U-Th)/He Thermochronology. *J. Anal. Chem.* **2005**, *60*, 1300–1307. [CrossRef]
7. Blackburn, T.J.; Stockli, D.F.; Walker, J.D. Magnetite (U-Th)/He Dating and Its Application to the Geochronology of Intermediate to Mafic Volcanic Rocks. *Earth Planet. Sci. Lett.* **2007**, *259*, 360–371. [CrossRef]
8. Yakubovich, O.V.; Vikentyev, I.V.; Zarubina, O.V.; Bryanskiy, N.V.; Gorokhovskii, B.M. U–Th–He Dating of Pyrite from the Uzelga Copper-Zinc Massive Sulfide Deposit (South Urals, Russia): First Application of a New Geochronometer. *Dokl. Earth Sci.* **2019**, *485*, 368–371. [CrossRef]
9. Yakubovich, O.; Podolskaya, M.; Vikentyev, I.; Fokina, E.; Kotov, A. U-Th-He Geochronology of Pyrite from the Uzelga VMS Deposit (South Urals)—New Perspectives for Direct Dating of the Ore-Forming Processes. *Minerals* **2020**, *10*, 629. [CrossRef]
10. Hnatyshin, D.; Creaser, R.A.; Meffre, S.; Stern, R.A.; Wilkinson, J.J.; Turner, E.C. Understanding the Microscale Spatial Distribution and Mineralogical Residency of Re in Pyrite: Examples from Carbonate-Hosted Zn-Pb Ores and Implications for Pyrite Re-Os Geochronology. *Chem. Geol.* **2020**, *533*, 119427. [CrossRef]
11. Stein, H.J.; Morgan, J.W.; Scherstén, A. Re-Os Dating of Low-Level Highly Radiogenic (LLHR) Sulfides: The Harnäs Gold Deposit, Southwest Sweden, Records Continental-Scale Tectonic Events. *Econ. Geol.* **2000**, *95*, 1657–1672. [CrossRef]
12. Christensen, J.N.; Halliday, A.N.; Leigh, K.E.; Randell, R.N.; Kesler, S.E. Direct Dating of Sulfides by RbSr: A Critical Test Using the Polaris Mississippi Valley-Type ZnPb Deposit. *Geochim. Cosmochim. Acta* **1995**, *59*, 5191–5197. [CrossRef]
13. Petke, T.; Diamond, L.W. Rb-Sr Dating of Sphalerite Based on Fluid Inclusion-Host a Clarification of Why It Works Mineral. *Econ. Geol.* **1996**, *91*, 951–956. [CrossRef]
14. Smith, P.E.; Evensen, N.M.; York, D.; Szatmari, P.; Oliveira, D.C. Single-Crystal Ar- 39 Ar Dating of Pyrite: No Fool' s Clock. *Geology* **2001**, *29*, 403–406. [CrossRef]
15. Ivanov, A.V.; Vanin, V.A.; Demonterova, E.I.; Gladkochub, D.P.; Donskaya, T.V.; Gorovoy, V.A. Application of the "no Fool's Clock" to Dating the Mukodek Gold Field, Siberia, Russia. *Ore Geol. Rev.* **2015**, *69*, 352–359. [CrossRef]
16. Yang, J.H.; Zhou, X.H. Rb-Sr, Sm-Nd, and Pb Isotopes Systematics of Pyrite: Implications for the Age and Genesis of Lode Gold Deposits. *Geology* **2002**, *29*, 711–714. [CrossRef]
17. Morelli, R.M.; Creaser, R.A.; Selby, D.; Kelley, K.D.; Leach, D.L.; King, A.R. Re-Os Sulfide Geochronology of the Red Dog Sediment-Hosted Zn-Pb-Ag Deposit, Brooks Range, Alaska. *Econ. Geol.* **2004**, *99*, 1569–1576. [CrossRef]
18. Lawley, C.; Selby, D.; Imber, J. Re-Os Molybdenite, Pyrite, and Chalcopyrite Geochronology, Lupa Goldfield, Southwestern Tanzania: Tracing Metallogenic Time Scales at Midcrustal Shear Zones Hosting Orogenic Au Deposits. *Econ. Geol.* **2013**, *108*, 1591–1613. [CrossRef]
19. Hnatyshin, D.; Creaser, R.A.; Wilkinson, J.J.; Gleeson, S.A. Re-Os Dating of Pyrite Confirms an Early Diagenetic Onset and Extended Duration of Mineralization in the Irish Zn-Pb Ore Field. *Geology* **2015**, *43*, 143–146. [CrossRef]
20. Ding, C.; Nie, F.; Bagas, L.; Dai, P.; Jiang, S.; Ding, C.; Liu, C.; Peng, Y.; Zhang, G.; Shao, G. Pyrite Re-Os and Zircon U-Pb Dating of the Tugurige Gold Deposit in the Western Part of the Xing'an-Mongolia Orogenic Belt, China and Its Geological Significance. *Ore Geol. Rev.* **2016**, *72*, 669–681. [CrossRef]
21. Mathur, R.; Mutti, L.; Barra, F.; Gold, D.; Smith, R.C.; Doden, A.; Detrie, T.; Ruiz, J.; McWilliams, A. Fluid Inclusion and Re-Os Isotopic Evidence for Hot, Cenozoic Mineralization in the Central Pennsylvanian Valley and Ridge Province. *Mineral. Petrol.* **2008**, *93*, 309–324. [CrossRef]
22. Jiang, S.H.; Bagas, L.; Liang, Q.L. Pyrite Re-Os Isotope Systematics at the Zijinshan Deposit of SW Fujian, China: Constraints on the Timing and Source of Cu-Au Mineralization. *Ore Geol. Rev.* **2017**, *80*, 612–622. [CrossRef]
23. Large, R.R.; Halpin, J.A.; Danyushevsky, L.V.; Maslennikov, V.V.; Bull, S.W.; Long, J.A.; Gregory, D.D.; Lounejeva, E.; Lyons, T.W.; Sack, P.J.; et al. Trace Element Content of Sedimentary Pyrite as a New Proxy for Deep-Time Ocean-Atmosphere Evolution. *Earth Planet. Sci. Lett.* **2014**, *389*, 209–220. [CrossRef]

24. Butler, I.B.; Nesbitt, R.W. Trace Element Distributions in the Chalcopyrite Wall of a Black Smoker Chimney: Insights from Laser Ablation Inductively Coupled Plasma Mass Spectrometry (LA-ICP-MS). *Earth Planet. Sci. Lett.* **1999**, *167*, 335–345. [CrossRef]

25. Baranov, E.N.; Vertepov, G.I. Concentration of Uranium in Sulphides as an Indicator of Possible Uranium Deposit. *At. Energy* **1966**, *20*, 170–171. [CrossRef]

26. Garuti, G.; Zaccarini, F. Minerals of Au, Ag and U in Volcanic-Rock-Associated Massive Sulfide Deposits of the Northern Apennine Ophiolite, Italy. *Can. Mineral.* **2005**, *43*, 935–950. [CrossRef]

27. Moloshag, V.P. Radioactive Mineralization of Supergene Ores of Sulfide Deposits of the Urals by the Example of the Tan'er Deposit. *Ezhegodnik* **2015**, *162*, 169–171.

28. Ayupova, N.R.; Melekestseva, I.Y.; Maslennikov, V.V.; Tseluyko, A.S.; Blinov, I.A.; Beltenev, V.E. Uranium Accumulation in Modern and Ancient Fe-Oxide Sediments: Examples from the Ashadze-2 Hydrothermal Sulfide Field (Mid-Atlantic Ridge) and Yubileynoe Massive Sulfide Deposit (South Urals, Russia). *Sediment. Geol.* **2018**, *367*, 164–174. [CrossRef]

29. Farley, K.A.; Wolf, R.A.; Silver, L.T. The Effects of Long Alpha-Stopping Distances on (U-Th)/He Ages. *Geochim. Cosmochim. Acta* **1996**, *60*, 4223–4229. [CrossRef]

30. Descostes, M.; Schlegel, M.L.; Eglizaud, N.; Descamps, F.; Miserque, F.; Simoni, E. Uptake of Uranium and Trace Elements in Pyrite (FeS$_2$) Suspensions. *Geochim. Cosmochim. Acta* **2010**, *74*, 1551–1562. [CrossRef]

31. Stuart, F.M.; Duckworth, R.; Turner, G.; Schofield, P.F. Helium and Sulfur Isotopes of Sulfide Minerals from Middle Valley. *Proc. Ocean Drill. Progr. Sci. Results* **1994**, *139*, 387–392.

32. Jean-Baptiste, P.; Fouquet, Y. Abundance and Isotopic Composition of Helium in Hydrothermal Sulfides from the East Pacific Rise at 13° N. *Geochim. Cosmochim. Acta* **1996**, *60*, 87–93. [CrossRef]

33. Bortnikov, N.S.; Vikentyev, I.V.; Stavrova, O.O.; Ikorskii, S.V.; Kamenskii, I.L.; Bogdanov, Y.A.; Avedisyan, A.A. Helium Isotopic Composition and Hydrocarbons in Fluid Inclusions from Serpentinites and Sulfides of the Logachev and Rainbow Hydrothermal Fields, Mid-Atlantic Ridge. *Dokl. Earth Sci.* **2000**, *375*, 1387–1390.

34. Bortnikov, N.; Ikorskii, S.; Kamenskii, I.; Avetisyan, A.; Simonov, V.; Bogdanov, Y.; Lein, A.; Sagalevich, A.; Vikentyev, I.; Stavrova, O. Modem Sulfide Ores at Mid-Atlantic Ridge and Pacific Back-Arc Basins: Fluid Inclusion, Hydrocarbon and He, Ar, and S Isotope Studies. In *Mineral Exploration and Sustainable Development*; Eliopoulous, D.G., Ed.; Millpress: Rotterdam, The Netherlands, 2003; pp. 115–118.

35. Luders, V.; Niedermann, S. Helium isotope composition of fluid inclusions hosted in massive sulfides from modern submarine hydrothermal systems. *Sci. Commun.* **2010**, *105*, 443–449. [CrossRef]

36. Andreev, A.V. Geological Structure, Conditions of Localization and Patterns of Formation of Gold Ores of the Novogodne-Monto Deposit (Polar Urals). *Geol. Miner. Geoecol. North-West Russ.* 2006; 7–9.

37. Puchkov, V.N. Geology of Urals and Cis–Urals. In *Actual Problems of Stratigraphy, Tectonics, Geodynamics and Metallogeny*; Design Poligraph Service Publ: Ufa, Russia, 2010.

38. Yazeva, R.G.; Bochkarev, V.V. *Voikar Volcanoplutonic Belt, Polar Urals*; Uralian Sci. Center USSR Acad. Sci.: Sverdlovsk, Ukraine, 1984.

39. Sobolev, I.D.; Soboleva, A.A.; Udoratina, O.V.; Kaneva, T.A.; Kulikova, K.V.; Vikentiev, I.V.; Khubanov, V.B.; Buyantuev, M.D.; Hourigan, J.K. First Results of U-Pb (LA-ICP-MS) Dating of Detrital Zircons from Paleozoic Island Arc Clastic Rocks of Polar Urals. *Bull. Moscow Soc. Nat. Geol. Ser.* **2017**, *92*, 3–26.

40. Sobolev, I.D.; Vikentyev, I.V.; Soboleva, A.; Travin, A.V. Results of U/Pb SIMS Dating of Zircons and 39Ar/40Ar Age of Plagioclase from Rocks of the Sob' Complex (Petropavlovsk Gold Deposit, Polar Urals). In Proceedings of the Conference Methods and Geological Results of Studying Isotopic Geochronometric Systems of Minerals and Rocks, Moscow, Russia, 5–8 February 2018; IGEM RAS: Moscow, Russia, 2018; pp. 398–401.

41. Sobolev, I.D.; Soboleva, A.A.; Udoratina, O.V.; Varlamov, D.A.; Hourigan, J.K.; Khubanov, V.B.; Buyantuev, M.D.; Soboleva, D.A. Devonian Island-Arc Magmatism of the Voikar Zone in the Polar Urals. *Geotectonics* **2018**, *52*, 531–563. [CrossRef]

42. Nalivkin, D.V. *Geolgical Map of USSR and Surrounding Territories*; Nedra Publishers: Leningrad, USSR, 1983.

43. Volchkov, A.; Girfanov, M.; Kryazhev, S.; Andreev, A.; Cheremsin, A.; Mansurov, R. *The Position of Gold Mineralization of the Toupugol-Khanmeyshor Ore Area in Ore-Containing Complexes, Their Mineral and Geochemical Characteristics and Comparison with the Reference Objects of the Novogodnee-Monto Mineralized Area*; unpublished report; Moscow, Russia, 2008.

44. Udoratina, O.V.; Kuznetsov, N.B. Sob' Plagiogranite Complex in the Polar Urals. *Byull. Mosk. O-va Ispyt. Prir. Otd. Geol.* **2007**, *82*, 49–59.

45. Vikentyev, I.V.; Mansurov, R.K.; Ivanova, Y.N.; Tyukova, E.E.; Sobolev, I.D.; Abramova, V.D.; Vykhristenko, R.I.; Trofimov, A.P.; Khubanov, V.B.; Groznova, E.O.; et al. Porphyry-Style Petropavlovskoe Gold Deposit, the Polar Urals: Geological Position, Mineralogy, and Formation Conditions. *Geol. Ore Depos.* **2017**, *59*, 482–520. [CrossRef]

46. Chernyaev, E.V.; Chernyaeva, E.I.; Sedelnikov, A.Y. Geology of Novogodnee-Monto Au-Skarn Deposit (Polar Urals). *Skarns Their Genes. Ore Miner.* **2005**, 131–137.

47. Silaev, V.I.; Khazov, A.F.; Sokerin, M.Y. Ovogodnee-Monto Gold Deposit at the Polar Urals. In *Petrology and Mineralogy of the northern Urals and Timan*; Inst KomiNTs UrO RAN: Syktyvkar, Russia, 2003; pp. 159–172.

48. Kuznetsov, N.B.; Romanyuk, T.V. Paleozoic Evolution of the Polar Urals: Voikar Basin with Oceanic Crust Has Existed No Less than 65 Ma. *Byull. Mosk. O-Va Ispyt. Prir.* **2014**, *89*, 56–70.

49. Kenig, V.V.; Butakov, K.V. Deposits of Ore Gold Novogodne-Monto and Petropavlovskoe - a New Gold-Ore Region in the Polar Urals. *Explor. Prot. Miner. Resour.* **2013**, *11*, 22–24.

50. Sobolev, I.D.; Vikentyev, I.V.; Travin, A.V.; Bortnikov, N.S. Carboniferous Magmatism in the Polar Urals. *Dokl. Earth Sci.* **2020**, *494*, 773–778. [CrossRef]

51. Vikentyev, I.; Vikent'eva, O.; Tyukova, E.; Nikolsky, M.; Ivanova, J.; Sidorova, N.; Tonkacheev, D.; Abramova, V.; Blokov, V.; Spirina, A.; et al. Noble Metal Speciations in Hydrothermal Sulphides. *Minerals* **2021**, *11*, 488. [CrossRef]

52. Soloviev, S.; Kryazhev, S.; Dvurechenskaya, S.S. Geology, Mineralization, Stable Isotope Geochemistry, and Fluid Inclusion Characteristics of the Novogodnee-Monto Oxidized Au-(Cu) Skarn and Porphyry Deposit, Polar Ural, Russia. *Miner. Depos.* **2013**, *48*, 603–627. [CrossRef]

53. Girfanov, M.; Volchkov, A.; Kryazhev, S.G.; Novikov, V. Gold-Iron Oxide Bearing Ore-Magmatic System of the Auerbakh–Novogodnee Volcano-Plutonic Belt, the Polar Urals. In Proceedings of the 33rd International Geological Congress, Oslo, Norway, 6–14 August 2008; p. 1.

54. Trofimov, A.P.; Lyuchkin, V.A.; Pivovarov, A.P.; Funtikov, B.V. Geological and Geochemical Model of the Novogodne-Monto Gold-Ore-Skarn Deposit in the Polar Urals. *Skarns Genes. Ore Miner.* **2005**, 102–107.

55. Dushin, V.A.; Serdyukova, O.P.; Malyugin, A.A.; Nikulina, I.A.; Kozmin, V.S.; Burmako, P.L.; Abaturova, I.V.; Kozmina, L.I. *State Geological Map of the Russian Federation, Scale 1: 200,000. (3rd Generation). Ser. Polar Ural, Sheet No. Q-42-VII, VIII (Obskoi), Explanatory Note*; VSEGEI: Saint Petersburg, Russia, 2014.

56. Bortnikov, N.S.; Vikentyev, I.V. Endogenous Metallogeny of the Urals. In *Mineral Deposit Research for a High-Tech World*; Jonsson, E., Ed.; Sverige AB: Uppsala, Sweden, 2013; pp. 1508–1511.

57. Ivanova, J.N.; Vyhristenko, R.I.; Vikentyev, I.V. Geological Position and Structural Control of Ore Mineralization in the Toupugol-Khanmeyshor District (the Polar Urals) Based on the Remote Sensing Results. *Izv. Atmos. Ocean. Phys.* **2019**, *55*, 1379–1388. [CrossRef]

58. Mansurov, R.K. Geological Structure of the Petropavlovsk Gold Deposit, Polar Urals. *Rudy Met* **2009**, *5*, 70–74.

59. Vikentyev, I.V.; Abramova, V.D.; Ivanova, Y.N.; Al, E. Trace Elements in Pyrite from the Petropavlovsk Gold–Porphyry Deposit (Polar Urals): Results of LA-ICP-MS Analysis. *Dokl. Earth Sci.* **2016**, *470*, 976–980. [CrossRef]

60. Vikentyev, I.V.; Sobolev, I.D.; A.V., T. First Results of 40Ar/39Ar Dating of Sericite from Metasomatites of the Petropavlovsk Gold Deposit in the Context of the Paleozoic Metallogeny of the Island-Arc System of the Polar Urals. *Metallog. Anc. Mod. Ocean.* **2019**, *25*, 185–189.

61. Yakubovich, O.V.; Shukolyukov, Y.A.; Kotov, A.B.; Brauns, M.; Samsonov, A.V.; Komarov, A.N.; Yakovleva, S.Z.; Sal'nikova, E.B.; Gorokhovskii, B.M. U-Th-He Dating of Native Gold: First Results, Problems, and Outlooks. *Petrology* **2014**, *22*, 429–437. [CrossRef]

62. Vermeesch, P. HelioPlot, and the Treatment of Overdispersed (U–Th–Sm)/He Data. *Chem. Geol.* **2010**, *271*, 108–111. [CrossRef]

63. Vermeesch, P. Three New Ways to Calculate Average (U-Th)/He Ages. *Chem. Geol.* **2008**, *249*, 339–347. [CrossRef]

64. Burnard, P.G.; Polya, D.A. Importance of Mantle Derived Fluids during Granite Associated Hydrothermal Circulation: He and Ar Isotopes of Ore Minerals from Panasqueira. *Geochim. Cosmochim. Acta* **2004**, *68*, 1607–1615. [CrossRef]

65. Ziegler, J.F.; Ziegler, M.D.; Biersack, J.P. SRIM—The Stopping and Range of Ions in Matter. *Nucl. Inst. Methods Phys. Res. B* **2010**, *268*, 1818–1823. [CrossRef]

66. Gautheron, C.; Tassan-Got, L.; Ketcham, R.A.; Dobson, K.J. Accounting for Long Alpha-Particle Stopping Distances in (U-Th-Sm)/He Geochronology: 3D Modeling of Diffusion, Zoning, Implantation, and Abrasion. *Geochim. Cosmochim. Acta* **2012**, *96*, 44–56. [CrossRef]

67. Vikentyev, I.V.; Belogub, E.V.; Novoselov, K.A.; Moloshag, V.P. Metamorphism of Volcanogenic Massive Sulphide Deposits in the Urals. Ore Geology. *Ore Geol. Rev.* **2017**, *85*, 30–63. [CrossRef]

68. Barrie, C.D.; Pearce, M.A.; Boyle, A.P. Reconstructing the Pyrite Deformation Mechanism Map. *Ore Geol. Rev.* **2011**, *39*, 265–276. [CrossRef]

69. Craig, J.R.; Vokes, F.M. The Metamorphism of Pyrite and Pyritic Ores: An Overview. *Mineral. Mag.* **1993**, *57*, 3–18. [CrossRef]

70. Mochalov, A.G.; Yakubovich, O.V.; Stuart, F.M.; Bortnikov, A.N.S. New Evidence of the Polycyclic Genesis of Platinum Placer-Forming Formations of the Kondyor Alkaline-Ultramafic Massif: Results of ^{190}Pt-^{4}He Dating. *Dokl. Earth Sci.* **2021**, *498*, 372–378. [CrossRef]

71. Remizov, D.N. *Island-Arc System of the Polar Urals: Petrology and Evolution of the Deep-Seated Zones*; UrO RAS: Ekaterinburg, Russia, 2004.

72. Andreichev, V.L. *Isotopic Geochronology of Ultramafic-Mafic and Granitoid Associations of the Eastern Slope of the Polar Urals*; Geoprint: Syktyvkar, Russia, 2004.

73. Udoratina, O.V.; Kuznetsov, N.B.; Matukov, D.I. Age of Granitoids of the Yanaslora Massif: U-Pb Data. Petrology of Magmatic and Metamorphic Complexes. *Mat. V Vseros. Conf. Tomsk TsNTI* **2005**, *5*, 135–142.

74. Ivanova, J.N.; Vykhristenko, R.I.; Vikentyev, V.I. Structural Control of Gold Mineralization of the Central Part of the Malouralsky Volcanic-Plutonic Belt (the Polar Urals) Based on the Analysis of Multispectral Images of the Landsat 8 Spacecraft. *Izv. Atmos. Ocean. Phys.* **2020**, *56*, 1537–1545. [CrossRef]